

Hybrid graded element model for transient heat conduction in functionally graded materials

Lei-Lei Cao · Qing-Hua Qin · Ning Zhao

Received: 13 October 2010 / Revised: 19 March 2011 / Accepted: 27 April 2011

©The Chinese Society of Theoretical and Applied Mechanics and Springer-Verlag Berlin Heidelberg 2012

Abstract This paper presents a hybrid graded element model for the transient heat conduction problem in functionally graded materials (FGMs). First, a Laplace transform approach is used to handle the time variable. Then, a fundamental solution in Laplace space for FGMs is constructed. Next, a hybrid graded element is formulated based on the obtained fundamental solution and a frame field. As a result, the graded properties of FGMs are naturally reflected by using the fundamental solution to interpolate the intra-element field. Further, Stefest's algorithm is employed to convert the results in Laplace space back into the time–space domain. Finally, the performance of the proposed method is assessed by several benchmark examples. The results demonstrate well the efficiency and accuracy of the proposed method.

Keywords Graded element model · Functionally graded materials · Hybrid FEM · Transient heat conduction

1 Introduction

Traditional composite materials are ineffective to satisfy spe-

cial requirements for working in harsh conditions, including high temperature and large temperature gradients, due to significant stress concentrations caused by their instantaneous and stepped variations in material properties. Functionally graded materials (FGMs) are a new generation of composite material whose microstructure varies from one material to another with a specific gradient. This smooth variation of material properties significantly improves the mechanical strength and fracture toughness of FGMs. Since FGMs are expected to be used in harsh thermal environments and in various working conditions, it is necessary to effectively analyze their transient heat conduction behavior. Investigation of transient heat conduction in FGMs is difficult because of the time-dependent excitation and spatial variations of their material properties.

For time-dependent problems, treatment of the time variable can essentially be classified into two categories [1]: the time domain approaches (usually a time-stepping scheme), which solve the problem directly in its time–space domain, and the transform space approaches (usually the Laplace transform, LT for short), which solve the problem in a transformed Laplace domain first and then convert the results back into the time–space domain. Time-stepping schemes always start from an initial time and provide the solution in the following time step, then take this solution as the new initial condition, conducting the solution procedure repeatedly. It should be mentioned that the disadvantage of time-stepping schemes is that they might be numerically inefficient and unstable. The LT is a powerful alternative that eliminates time derivatives by transforming the original heat conduction equation into one in Laplace space. However, once the new equation is solved in Laplace space, an inverse transform is required to obtain the solution in the time–space domain. Therefore the accuracy of the solution relies on an efficient and accurate numerical inverse transform [2].

Alibeigloo [3] derived a steady-state solution of temperature field for a square exponential FGMs. It is, however,

L.-L. Cao
Key Laboratory for Road Construction Technology
& Equipment of MOE,
Chang'an University, 710064 Xi'an, China

L.-L. Cao · Q.-H. Qin (✉)
Research School of Engineering,
Australian National University,
Canberra, ACT, 0200, Australia
e-mail: qinghua.qin@anu.edu.au

N. Zhao
School of Mechatronics,
Northwestern Polytechnical University,
710072 Xi'an, China

difficult to obtain exact transient solution of FGMs, so various numerical algorithms have been developed in the past decades for heat conduction problems in FGMs. Among them, the boundary element method (BEM) is a very popular method which relies on the actual Green's function (GF) associated with the function describing the material gradation. Most existing research has used an exponential law for FGMs. Gray et al. [4] and Berger et al. [5] derived the GF for isotropic and anisotropic FGMs, respectively, in steady-state heat conduction problems. Paulino [6] introduced a Galerkin BEM for FGMs. Sutradhar et al. [2] extended the above work to transient heat conduction problems by using Laplace transform boundary element method (LTBEM), and then proposed a simple BEM which can be used to solve transient heat conduction problems for a broad range of FGMs (quadratic, exponential and trigonometric) [7]. Sladek et al. [8, 9] presented a local boundary integral equation formulation for transient heat conduction in exponential FGMs. In addition, the method of fundamental solution (MFS) has also been developed for FGMs. Marin applied MFS to steady-state heat conduction in FGMs [10] and also nonlinear FGMs [11]. Wang et al. [12] developed a meshless model for transient heat conduction of FGMs. Beside the well-established BEM and MFS, the finite element method (FEM) provides an effective alternative in numerical algorithms. Two typical finite element models can be found in the literature to simulate the physical behavior of FGMs: the stepwise constant model [13, 14] and the graded finite element model [15–17]. In the first model, the element rows are aligned with the gradient direction, the property of each row of homogeneous elements is taken to be the property at the centroid of the element, and the material gradient is achieved by a highly refined mesh. In the second model, the material gradient is directly sampled by assigning corresponding material properties at the Gauss integration points.

To improve the efficiency of FEM for solving transient heat conduction in FGMs, a new hybrid graded element model is developed in this paper, which builds upon the hybrid finite element formulation with fundamental solutions as internal interpolation functions (HFS-FEM) recently proposed by Wang and Qin [18] and incorporate with LT. It is capable of effectively modeling transient heat conduction in various FGMs. Unlike the hybrid Trefftz FEM (HT-FEM) [19], HFS-FEM uses fundamental solutions as internal interpolation functions, and thus inherits all the advantages of HT-FEM over conventional FEM and BEM (see Refs. [20–22]) and also avoids the difficulty encountered in constructing and selecting T-functions in HT-FEM [23]. For the hybrid graded element model, a linear combination of the fundamental solutions for FGMs at different source points is used to approximate the field variable within the element, and an independent frame field defined along the element boundary is employed to guarantee inter-element continuity. A variational functional is used to generate the final stiffness equation and establish a linkage between the boundary frame

field and the internal field at the element level. The proposed graded element formulation can incorporate the graded material properties at the element level, so it is more intuitive than the conventional homogeneous elements model and the Gauss point sampling model mentioned above in representing graded material properties. In the proposed model, the LT is used to eliminate time derivatives in the basic equations. After solving the problem by the hybrid graded element model in Laplace space, the Stehfest numerical inversion method is applied to obtain the solution in the time-space domain. It should be noted that although the same fundamental solution as in the BEM is employed, the proposed approach can avoid the singular or hyper-singular integrals encountered in BEM due to placing source points outside the element domain. Moreover, the element based model can manage complex shapes much better than meshless methods.

This paper begins with a description of basic formulations of transient heat conduction problems in Sect. 2. Then, the hybrid graded element model is described in Sect. 3, followed by numerical implementation of the inversion LT, as given in Sect. 4. Several benchmark examples are presented in Sect. 5, and conclusions are finally drawn in Sect. 6.

2 Basic formulations

2.1 Statement of heat conduction problems in FGMs

Consider a two-dimensional (2D) transient heat conduction problem

$$\nabla \cdot (k(X)\nabla u(X, t)) = \rho(X)c(X)\frac{\partial u(X, t)}{\partial t}, \quad (1)$$

with the following boundary conditions:

Dirichlet boundary condition

$$u(X, t) = \bar{u}(X, t), \quad \text{on } \Gamma_u. \quad (2)$$

Neumann boundary condition

$$q(X, t) = \bar{q}(X, t), \quad \text{on } \Gamma_q, \quad (3)$$

where t denotes the time variable ($t > 0$), k is the thermal conductivity dependent on the special variables $X \in \Omega \subset \mathbf{R}^d$, d is the number of dimensions of the solution domain Ω ($d = 2$ in this study), ρ is the mass density, c is the specific heat, and u is the unknown temperature field, q represents the boundary heat flux defined by $q = -k\partial u/\partial n$, where n is the unit outward normal to the boundary $\Gamma = \Gamma_u \cup \Gamma_q$, \bar{u} and \bar{q} are specified temperature and heat flow, respectively, on the related boundaries. In addition, an initial condition must be given for the time dependent problem. In this paper, a zero initial temperature distribution is considered, i.e.

$$u(X, 0) = u_0(X) = 0. \quad (4)$$

The composition and the volume fraction of FGMs constituents vary gradually with coordinate X , giving a non-uniform microstructure with continuously graded macro-properties (conductivity, specific heat, density). In the

present work, to make the derivation tractable, the mass density is assumed to be constant within each element and taken the value of ρ at the centroid of the element. The thermal conductivity and specific heat have been chosen to have the same functional variation so that the thermal diffusivity η is constant, that is

$$k(X) = k_0 f(X), \tag{5}$$

$$c(X) = c_0 f(X), \tag{6}$$

and

$$\eta = \frac{k_0}{c_0 \rho}. \tag{7}$$

It should be mentioned that the above assumption in FGMs leads to a class of solvable problems and can provide benchmark solutions to other numerical methods, such as FEM, meshless and BEM. Moreover, it can provide valuable insight into the thermal behavior of FGMs [7]. So this assumption has been followed by a lot of researchers in solving transient thermal problems in FGMs, see Refs. [2, 7–9, 12, 24].

2.2 LT and fundamental solution in Laplace space

The LT of a function $u(X, t)$ is defined by

$$L(u(X, t)) = U(X, s) = \int_0^\infty u(X, t)e^{-st} dt, \tag{8}$$

where s is the Laplace parameter. By integration by parts, one can show that

$$L\left[\frac{\partial u(X, t)}{\partial t}\right] = sU(X, s) - u_0(X). \tag{9}$$

The boundary conditions (2) and (3) become

$$U(X, s) = \frac{\bar{u}(X, t)}{s}, \quad \text{on } \Gamma_u, \tag{10}$$

$$P(X, s) = \frac{\bar{q}(X, t)}{s}, \quad \text{on } \Gamma_q. \tag{11}$$

2.2.1 Exponentially graded material

First, we consider an FGMs with thermal conductivity and specific heat varying exponentially in one Cartesian coordinate, X_2 , only

$$k(X_2) = k_0 e^{2\beta X_2}, \tag{12}$$

$$c(X_2) = c_0 e^{2\beta X_2}, \tag{13}$$

where β is the non-homogeneity graded parameter.

Substituting Eqs. (12) and (13) into Eq. (1) yields

$$\nabla^2 u + 2\beta u_{X_2} = \frac{1}{\eta} \frac{\partial u}{\partial t}, \tag{14}$$

where u_{X_2} denotes the derivative of u with respect to X_2 ($u_{X_2} = \partial u / \partial X_2$).

After performing the LT, Eq. (14) becomes

$$\nabla^2 U + 2\beta U_{X_2} - \frac{s}{\eta} U = 0, \tag{15}$$

in LT space, where $u_0(X) = 0$ (at $t = 0$) is considered (see Eq. (4)).

To obtain the fundamental solution of Eq. (15), the following substitution is used here

$$U = e^{-\beta X_2} G. \tag{16}$$

In this case, the differential Eq. (15) in Laplace space becomes

$$\nabla^2 G - \left(\beta^2 + \frac{s}{\eta}\right) G = 0. \tag{17}$$

Obviously, Eq. (17) is the modified Helmholtz equation, whose fundamental solution is

$$G = \frac{1}{2\pi} K_0\left(\sqrt{\beta^2 + \frac{s}{\eta}} r\right). \tag{18}$$

Making use of Eq. (16), we obtain the fundamental solution of Eq. (15) in Laplace space

$$N(X, X_S) = \frac{1}{2\pi} e^{-\beta(X_2 - X_{S2})} K_0\left(\sqrt{\beta^2 + \frac{s}{\eta}} r\right), \tag{19}$$

where $r = \|X - X_S\|$, X and X_S denote arbitrary field point and source point in the infinite domain, respectively. K_0 is the modified zero order Bessel function of the second kind.

2.2.2 General method for FGMs with different variation of properties

The method can be extended by variable transformations [7] to a broader range of FGMs, not only exponential but also quadratic and trigonometric material variation. By defining a variable [7]

$$v(X, t) = \sqrt{k(X)} u(X, t). \tag{20}$$

Equation (1) can be rewritten as

$$\nabla^2 v + \left[\frac{\nabla k(X) \cdot \nabla k(X)}{4k^2(X)} - \frac{\nabla^2 k(X)}{2k(X)}\right] v = \frac{\rho c(X)}{k(X)} \frac{\partial v}{\partial t}. \tag{21}$$

For simplicity, define

$$k'(X) = \frac{\nabla k(X) \cdot \nabla k(X)}{4k^2(X)} - \frac{\nabla^2 k(X)}{2k(X)}. \tag{22}$$

Then, Eq. (21) can be rewritten as

$$\nabla^2 v + k'(X)v = \frac{1}{\eta} \frac{\partial v}{\partial t}. \tag{23}$$

After performing the LT, the differential equation (23) becomes

$$\nabla^2 V + k'V - \frac{s}{\eta} V = 0. \tag{24}$$

When k' is a constant, Eq. (24) is a modified Helmholtz equation whose fundamental solution is known. Then the fundamental solution of Eq. (1) in Laplace space can be obtained by inverse transformation

$$N(X, X_S) = \frac{1}{2\pi} \frac{K_0\left(\sqrt{-k' + \frac{s}{\eta}} r\right)}{k(X)^{1/2} k(X_S)^{1/2}}. \tag{25}$$

For quadratic material

$$k(X) = k_0(a_1 + \beta X_2)^2. \tag{26}$$

In this case, $k' = 0$ in Eq. (24).

For trigonometric material

$$k(X) = k_0(a_1 \cos \beta X_2 + a_2 \sin \beta X_2)^2. \tag{27}$$

In this case, $k' = \beta^2$ in Eq. (24).

For exponential material

$$k(X) = k_0(a_1 e^{\beta X_2} + a_2 e^{-\beta X_2})^2. \tag{28}$$

In this case, $k' = -\beta^2$ in Eq. (24). By substituting $k' = -\beta^2$ into Eq. (25) and using the exponential law, the fundamental solution given by Eq. (25) is reduced to Eq. (19). Note that for quadratic, trigonometric and exponential variations of both heat conductivity and specific heat, the FGMs transient problem can be transformed into the same differential equation which has a simple and standard form as shown by Eq. (23) [7].

3 Generation of graded element

In this section, an element formulation is presented to deal with materials with continuous variation of physical properties. Such an element model is usually known as a hybrid graded element, and can be used for solving the boundary value problem (BVP) in Laplace space. The governing equation is the transformed governing equation of Eq. (1) in Laplace space. The corresponding boundary conditions are defined in Eqs. (10) and (11).

The proposed approach is based on a hybrid finite element formulation in which fundamental solutions are taken as internal interpolation functions (HFS-FEM) [18]. As in HT-FEM, the main idea of HFS-FEM is to establish an appropriate hybrid FE formulation, in which intra-element continuity is enforced on a nonconforming internal field formed by a linear combination of fundamental solutions at points outside the element domain under consideration, while an auxiliary frame field is independently defined on the element boundary to enforce field continuity across the inter-element boundaries. But unlike HT FEM, the intra-element fields are constructed based on the fundamental solution, rather than T-functions. Consequently, a variational functional corresponding to the new trial function is required to derive the related stiffness matrix equation. As in conventional FEM, the solution domain is divided into sub-domains or elements. For a particular element, say element e , its domain is denoted by Ω_e and bounded by Γ_e . Since a nonconforming function is used for modeling the internal fields, additional continuities are usually required in the proposed hybrid FE approach for the common boundary Γ_{lef} between any two adjacent elements “ e ” and “ f ” (see Fig. 1) [25]

$$\begin{aligned} \text{conformity : } & U_e = U_f, \\ \text{reciprocity : } & P_e + P_f = 0, \end{aligned} \quad \text{on } \Gamma_{lef} = \Gamma_e \cap \Gamma_f. \tag{29}$$

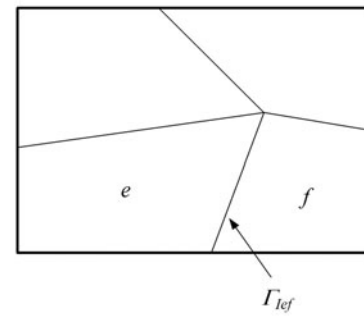


Fig. 1 Illustration of continuity between two adjacent elements “ e ” and “ f ”

3.1 Non-conforming intra-element field

For a particular element, say element e , which occupies a sub-domain Ω_e , the field variable within the element is extracted from a linear combination of fundamental solutions centered at different source points (see Fig. 2), that is

$$U_e(x) = \sum_{j=1}^{n_s} N_e(x, x_S) c_{ej} = N_e(x) c_e, \tag{30}$$

$$\forall x \in \Omega_e \subset \mathbf{R}^d, \quad x_S \notin \Omega_e,$$

where c_{ej} is undetermined coefficients and n_s is the number of virtual sources outside the element e . $N_e(x, x_S)$ is the required fundamental solution expressed in local element coordinates (x_1, x_2) , rather than global coordinates (X_1, X_2) (see Fig. 2). Clearly, Eq. (30) analytically satisfies the transformed governing equation of Eq. (1) in Laplace space due to the inherent property of $N_e(x, x_S)$.

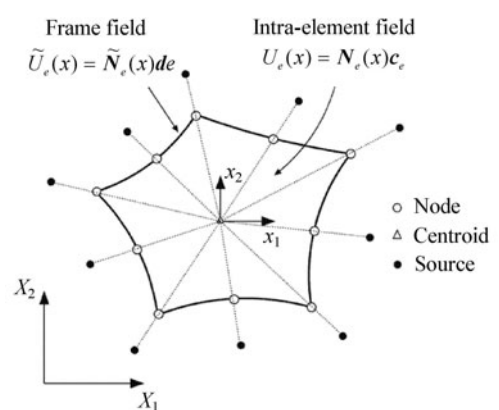


Fig. 2 Intra-element field, frame field in a particular element in HFS-FEM, and the generation of source points for a particular element

The fundamental solution for FGMs (N_e in Eq. (30)) is used to approximate the intra-element field for an FGMs. The smooth variation of material properties throughout an element can be achieved by using the fundamental solution

which can reflect the impact of a concentrated unit source acting at a point on any other points. The model inherits the essence of an FGMs, so it can simulate FGMs more naturally than the stepwise constant approximation, which has been frequently used in conventional FEM. Figure 3 illustrates the difference between the two models when the thermal conductivity varies along direction X_2 .

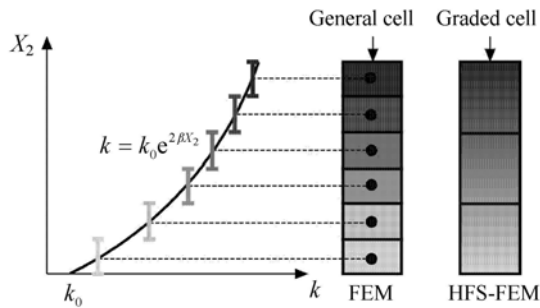


Fig. 3 Comparison of computational cells in conventional FEM and the proposed HFS-FEM

Note that the thermal conductivity in Eq. (1) is defined in the global coordinate system. When contriving the intra-element field for each element, this formulation must be transferred into the local element coordinate system defined at the center of the element, and the graded heat conductivity $k(X)$ in Eq. (5) can then be expressed by

$$k_e(X) = k_C(X)f(X), \tag{31}$$

for a particular element e , where $k_C(X)$ denotes the value of conductivity at the centroid of each element and can be calculated as

$$k_C(X) = k_0f(X_C), \tag{32}$$

where X_C is the global coordinates of the element centroid.

Accordingly, k_C is used to replace k (see Eq. (25)) in the formulation of the fundamental solution for the FGMs and to construct the intra-element field in the local element coordinate system for each element.

In practice, the generation of virtual sources is usually achieved by means of the following formulation employed in the MFS [12]

$$y = x_b + \gamma(x_b - x_c), \tag{33}$$

where γ is a dimensionless coefficient, x_b and x_c are, respectively, boundary point and geometrical centroid of the element. For a particular element shown in Fig. 2, we can use the nodes of the element to generate related source points for simplicity.

The corresponding normal heat flux on Γ_e is given by

$$P_e = -k_e \frac{\partial U_e}{\partial X_j} n_i = \mathbf{Q}_e \mathbf{c}_e, \tag{34}$$

where

$$\mathbf{Q}_e = -k_e \frac{\partial \mathbf{N}_e}{\partial X_j} n_i = -k_e \mathbf{A} \mathbf{T}_e, \tag{35}$$

with

$$\mathbf{T}_e = [\mathbf{N}_{e,1} \quad \mathbf{N}_{e,2}]^T, \quad \mathbf{A} = [n_1 \quad n_2]. \tag{36}$$

3.2 Auxiliary conforming frame field

In order to enforce conformity on the field variable U , for instance, $U_e = U_f$ on $\Gamma_e \cap \Gamma_f$ of any two neighboring elements e and f , an auxiliary inter-element frame field \tilde{U} is used and expressed, in terms of nodal degrees of freedom (DOF), \mathbf{d} , as used in conventional FEM, as

$$\tilde{U}_e(x) = \tilde{\mathbf{N}}_e(x) \mathbf{d}_e, \tag{37}$$

which is independently assumed along the element boundary, where $\tilde{\mathbf{N}}_e$ represents the conventional FE interpolating functions. For example, a simple interpolation of the frame field on the side with three nodes of a particular element can be given in the form of

$$\tilde{U} = \tilde{N}_1 \Psi_1 + \tilde{N}_2 \Psi_2 + \tilde{N}_3 \Psi_3, \tag{38}$$

where \tilde{N}_i ($i = 1, 2, 3$) stands for shape functions which are the same as those used in conventional FEM.

3.3 Modified variational and stiffness equation

With the intra-element field and the frame field independently defined in a particular element (see Fig. 2), the element stiffness equation can be generated through a variational approach. Here we just present the results directly; details of the derivation can be found in Refs. [17, 19].

The final functional defined only on the element boundary is

$$\Pi_{me} = -\frac{1}{2} \int_{\Gamma_e} P U d\Gamma - \int_{\Gamma_{qe}} \frac{\bar{q}}{s} \tilde{U} d\Gamma + \int_{\Gamma_e} P \tilde{U} d\Gamma. \tag{39}$$

Substituting Eqs. (30), (34) and (37) into the functional (39), yields

$$\Pi_e = -\frac{1}{2} \mathbf{c}_e^T \mathbf{H}_e \mathbf{c}_e - \mathbf{d}_e^T \mathbf{g}_e + \mathbf{c}_e^T \mathbf{G}_e \mathbf{d}_e, \tag{40}$$

where

$$\begin{aligned} \mathbf{H}_e &= \int_{\Gamma_e} \mathbf{Q}_e^T \mathbf{N}_e d\Gamma, \\ \mathbf{G}_e &= \int_{\Gamma_e} \mathbf{Q}_e^T \tilde{\mathbf{N}}_e d\Gamma, \\ \mathbf{g}_e &= \int_{\Gamma_{qe}} \tilde{\mathbf{N}}_e^T \frac{\bar{q}}{s} d\Gamma. \end{aligned} \tag{41}$$

Next, to enforce inter-element continuity on the common element boundary, the unknown vector \mathbf{c}_e must be expressed in terms of nodal DOF \mathbf{d}_e . The minimization of the functional Π_e with respect to \mathbf{c}_e and \mathbf{d}_e , respectively, yields

$$\frac{\partial \Pi_e}{\partial \mathbf{c}_e^T} = -\mathbf{H}_e \mathbf{c}_e + \mathbf{G}_e \mathbf{d}_e = \mathbf{0},$$

$$\frac{\partial \Pi_e}{\partial \mathbf{d}_e^T} = \mathbf{G}_e^T \mathbf{c}_e - \mathbf{g}_e = \mathbf{0},$$
(42)

from which the optional relationship between \mathbf{c}_e and \mathbf{d}_e , and the stiffness equation can be produced in the form of

$$\mathbf{c}_e = \mathbf{H}_e^{-1} \mathbf{G}_e \mathbf{d}_e, \quad \mathbf{K}_e \mathbf{d}_e = \mathbf{g}_e,$$
(43)

where $\mathbf{K}_e = \mathbf{G}_e^T \mathbf{H}_e^{-1} \mathbf{G}_e$ stands for the element stiffness matrix.

4 Numerical inversion of LT

In this section, we present a brief review of the inversion of the LT used in this work. In general, once the solution for $U(X, s)$ in the Laplace space is found numerically by the method proposed above, inversion of the LT is needed to obtain the solution for $u(X, t)$ in the original physical domain. There are many inversion approaches for LT algorithms available in Ref. [2]. A comprehensive review on those approaches can be found in Ref. [26]. In terms of numerical accuracy, computational efficiency and ease of implementation, Davies and Martin showed that Stehfest’s algorithm gives good accuracy with a fairly wide range of functions [1]. Therefore, Stehfest’s algorithm is chosen in our study.

If $F(s)$ is the LT of $f(t)$, an approximate value f_a of the function $f(t)$ for a specific time $t = T$ is given by

$$f_a = \frac{\ln 2}{T} \sum_{i=1}^N V_i F\left(\frac{\ln 2}{T} i\right),$$
(44)

where

$$V_i = (-1)^{N/2+i} \times \sum_{k=\frac{i-1}{2}}^{\min(i, N/2)} \frac{k^{N/2} (2k)!}{(N/2 - k)! k! (k-1)! (i-k)! (2k-i)!},$$
(45)

in which N must be taken as an even number. In implementation, one should compare the results for different N ’s to investigate whether the function is smooth enough, and determine an optimum N ’s [2]. Stehfest suggested $N = 10$ and other researchers have found no significant change for $6 \leq N \leq 10$ [1]. Therefore, $N = 10$ is adopted here. That means that for each specific time T it is necessary to solve different boundary value problems with corresponding Laplace parameters $s = (\ln 2/T)i, i = 1, 2, \dots, 10$, ten times in Laplace space, then weight and sum the solutions obtained in Laplace space.

5 Numerical assessment

To assess the performance of the proposed approach, it is desirable to select several benchmark problems which have

analytical solutions and are often used by researchers [7, 8] for transient heat conduction in FGMs. The convergence performance and sensitivity to mesh distortion of the proposed method are also investigated in this section. These examples cover the cases of functional graded plate with a range of functional material variations: exponential law in Example 1, quadratic law in Example 3, trigonometric law in Example 4; also, exponentially graded annulus sector in Example 2, and an L-shaped FGMs plate in Example 5. The results are compared with those obtained from analytical solution or the FEM software ANSYS.

Example 1

An exponentially graded plate is considered in this example. The thermal conductivity and specific heat are defined as $k = k_0 e^{2\beta X_2}$ and $c = c_0 e^{2\beta X_2}$, respectively. In the computation, $k_0 = 17 \text{ W/(m}\cdot\text{K)}$, $c_0 = 1.0 \text{ MJ/(kg}\cdot\text{K)}$, and the side length of the plate is $L = 0.04 \text{ m}$. On the two opposite sides parallel to the X_1 axis, two different temperatures are prescribed. As shown in Fig 4, one side is maintained at zero and the temperature of the other side is modified as described by the Heaviside function of $u = T \cdot H(t)$ with $T = 1^\circ\text{C}$ [8]. On the lateral sides of the plate the heat flux vanishes. 4×4 8-node quadrilateral elements are employed for the square domain. The analytical solution is [7]

$$u = T \frac{1 - e^{-2\beta X_2}}{1 - e^{-2\beta L}} + \sum_{n=1}^{\infty} \frac{2T e^{\beta L} n\pi \cos n\pi}{\beta^2 L^2 + n^2 \pi^2} \times \sin \frac{n\pi X_2}{L} e^{-\beta X_2} e^{-\left(\frac{n^2 \pi^2}{L^2} + \beta^2\right) \eta t}.$$
(46)

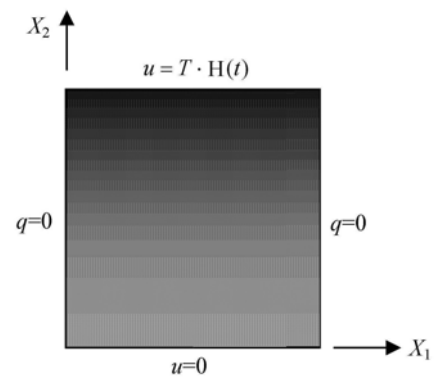


Fig. 4 Square functionally graded plate and boundary condition

Table 1 presents the temperature along X_2 -axis at $t = 20 \text{ s}$ ($\beta = 25$). It can be seen that the proposed method can achieve high accuracy. Figure 5 shows the temperature history at position $X_2 = 0.02 \text{ m}$ with four different graded parameters $\beta = 0, 10, 25, 50$. The numerical results are in excellent agreement with the analytical results. Also, as expected, with an increase in the value of β , a higher temperature at the position of interest is obtained in a longer period of time.

Table 1 Comparison of results along $X_2(\beta = 25, t = 20\text{ s})$

| X_2 | 0 | 0.005 | 0.010 | 0.015 | 0.020 | 0.025 | 0.030 | 0.035 | 0.040 |
|-----------------|---|---------|---------|---------|---------|---------|---------|---------|---------|
| Analytical | 0 | 0.203 2 | 0.369 3 | 0.511 2 | 0.636 4 | 0.748 0 | 0.846 3 | 0.930 6 | 1.000 0 |
| Proposed method | 0 | 0.202 7 | 0.368 6 | 0.510 7 | 0.636 1 | 0.747 8 | 0.846 2 | 0.930 6 | 1.000 0 |

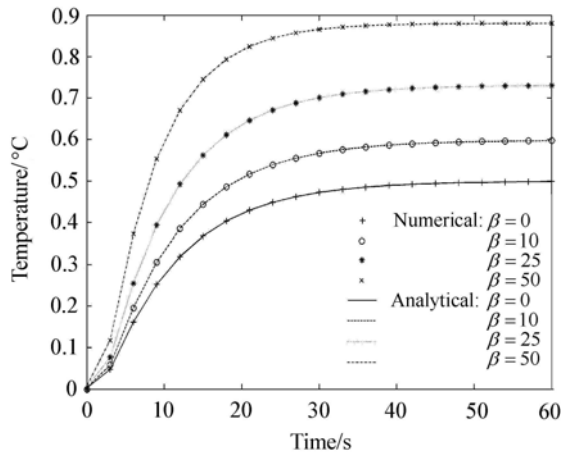


Fig. 5 Temperature history at position $X_2 = 0.02\text{ m}$ for an exponentially graded plate

The analytical solution for the final steady state is [3]

$$u = T \frac{e^{-2\beta X_2} - 1}{e^{-2\beta L} - 1} \left(u \rightarrow T \frac{X_2}{L} \text{ with } \beta \rightarrow 0 \right). \quad (47)$$

The results for the stationary or static loading conditions are presented in Fig. 6. The numerical results are in good agree-

ment with the analytical results for the steady state case. Table 2 presents the temperature history obtained by proposed method at another particular position $X_2 = 0.01\text{ m}$ and comparison is made with analytical solutions. From Table 2 we can see clearly that the proposed method is very efficient in solving transient problems.

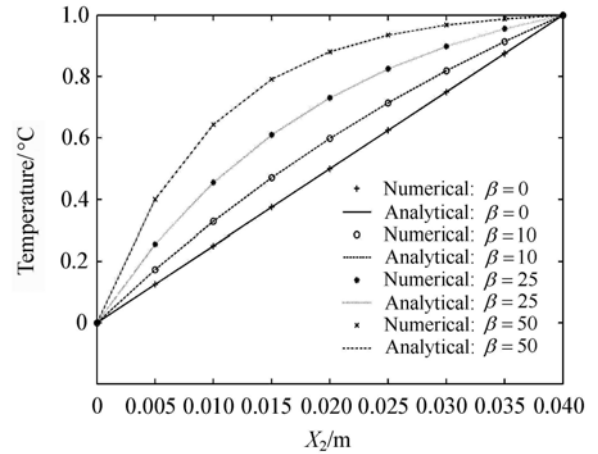


Fig. 6 Temperature distribution along X_2 for an FGMs plate under steady-state loading conditions

Table 2 Comparison of results from various methods at $X_2 = 0.01\text{ m} (\beta = 25)$

| | $t = 10\text{ s}$ | $t = 20\text{ s}$ | $t = 30\text{ s}$ | $t = 40\text{ s}$ | $t = 50\text{ s}$ | $t = 60\text{ s}$ | $t = \infty$ |
|-----------------|-------------------|-------------------|-------------------|-------------------|-------------------|-------------------|--------------|
| Analytical | 0.191 3 | 0.369 3 | 0.428 0 | 0.446 5 | 0.452 4 | 0.454 2 | 0.455 1 |
| Proposed method | 0.190 9 | 0.368 4 | 0.427 6 | 0.446 7 | 0.452 8 | 0.454 7 | 0.455 1 |

Example 2

An annulus sector domain is considered, with its boundary conditions shown in Fig. 7. The thermal conductivity and specific heat are graded along direction X_2 , and $k = k_0 e^{2\beta X_2}$, $c = c_0 e^{2\beta X_2}$ and $k_0 = 17\text{ W/(m}\cdot\text{K)}$, $c_0 = 1.0\text{ MJ/(kg}\cdot\text{K)}$ are used in the calculation. The inner and outer radii are assumed to be $R_1 = 0.08\text{ m}$ and $R_2 = 0.1\text{ m}$. 8-node quadrilateral elements are employed to model the solution domain and 4 elements are used to discretize along the radial direction (see Fig. 7). The special case with exponential parameter $\beta = 0$ corresponds to a homogeneous material. The analytical solution for the homogeneous case is [26]

$$u = \frac{T \ln(r/R_1)}{\ln(R_2/R_1)} - \pi \sum_{n=1}^{\infty} e^{-\eta \alpha_n^2 t} \frac{1}{F(\alpha_n)} \times T J_0(R_2 \alpha_n) J_0(R_1 \alpha_n) C_0(r, \alpha_n), \quad (48)$$

where

$$F(\alpha_n) = J_0(R_1 \alpha_n)^2 - J_0(R_2 \alpha_n)^2, \quad (49)$$

$$C_0(r, \alpha_n) = J_0(r \alpha_n) Y_0(R_1 \alpha_n) - Y_0(r \alpha_n) J_0(R_1 \alpha_n), \quad (50)$$

and α_n are roots of the transcendental equation

$$J_0(\alpha_n R_1) Y_0(\alpha_n R_2) - Y_0(\alpha_n R_1) J_0(\alpha_n R_2) = 0. \quad (51)$$

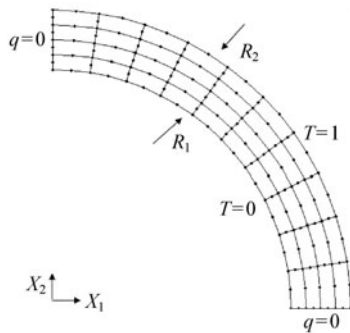


Fig. 7 Illustration of boundary condition and mesh division for the quarter domain

Figure 8 presents the temperature history at one particular point. The excellent agreement between the analytical and the numerical results can be seen in Fig. 8. To investigate the influence of the graded parameter, the calculation is also performed for $\beta = 10, 25, 50$, and the results at the particular point (0.09 m, 0) are shown in Fig. 9. Similar results can be observed as seen in the first example, in which the temperature increases with increasing graded parameter.

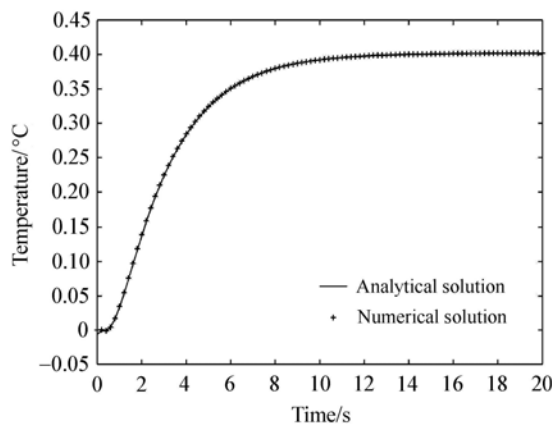


Fig. 8 Time variation of temperature at point (0.0875 m, 0) in the annulus sector with homogeneous material properties

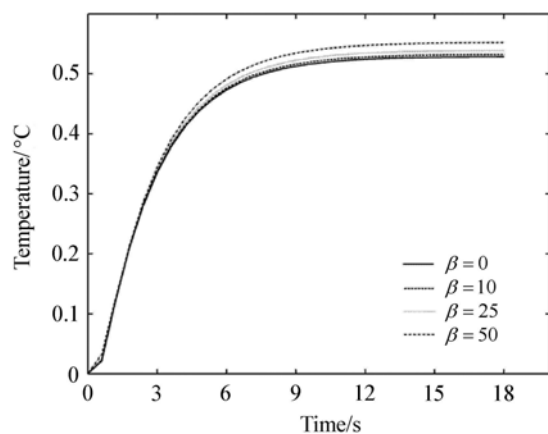


Fig. 9 Time variation of temperature at point (0.09 m, 0) in the FGMs annulus sector

Example 3

A quadratically graded square plate is considered in this example. The thermal conductivity and specific heat are defined as $k(X) = k_0(1 + \beta X_2)^2$ and $c(X) = c_0(1 + \beta X_2)^2$ ($\beta = 25$). The size of the plate, boundary condition, parameters and element discretization are the same as adopted in Example 1. The analytical solution is

$$u = \frac{T_1 X_2}{\sqrt{kL}} + \frac{2T_1}{\sqrt{k}} \sum_{n=1}^{\infty} \frac{\cos n\pi}{n\pi} \sin \frac{n\pi X_2}{L} e^{-\left(\frac{n^2 \pi^2}{L^2} \eta t\right)}, \tag{52}$$

where $T_1 = \sqrt{k_0}(1 + \beta L)T$.

The temperature distribution along X_2 -axis at different times is plotted in Fig. 10. Good agreement between the numerical and the analytical results is observed from Fig. 10.

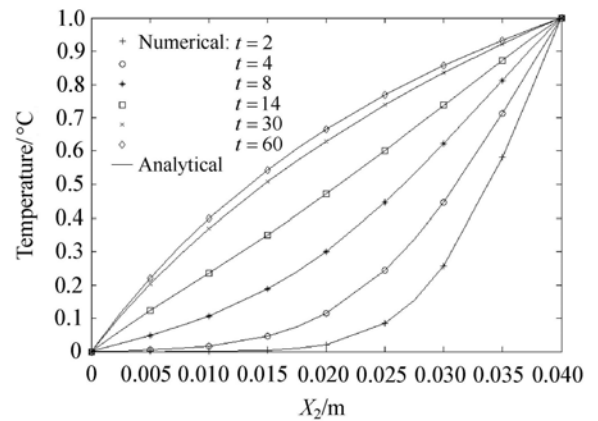


Fig. 10 Temperature distribution along X_2 at different times for the quadratically graded plate

To investigate the convergence of the proposed method, the calculation is also conducted for a series of meshes of $N \times N$ elements. In addition, to facilitate a quantitative understanding of the results, the average relative error of a variable f is introduced as $A_{re}(f) = \sqrt{\frac{\sum_{i=1}^N (f_{num} - f_{ana})_i^2}{\sum_{i=1}^N (f_{ana})_i^2}}$. It

can be seen from Table 3 that the relative error decreases along with refinement of the element meshes. The proposed method also gradually approximates the analytical solution with an increase in time.

Example 4

A trigonometrically graded square plate is considered in this example. The thermal conductivity and specific heat are defined as $k(X) = k_0(\cos \beta X_2 + \sin \beta X_2)^2$ and $c(X) = c_0(\cos \beta X_2 + \sin \beta X_2)^2$ ($\beta = 25$). Again, the size of the plate, boundary condition, parameters and element discretization

Table 3 Variation of average relative error with mesh density and time

| | 2 × 2 | 4 × 4 | 8 × 8 |
|----------|-------------------------|-------------------------|-------------------------|
| $t = 2$ | 2.6240×10^{-2} | 1.6912×10^{-2} | 4.6038×10^{-3} |
| $t = 20$ | 1.7934×10^{-2} | 4.2965×10^{-3} | 1.0230×10^{-3} |
| $t = 40$ | 1.2758×10^{-2} | 3.0528×10^{-3} | 7.5597×10^{-4} |
| $t = 60$ | 1.2149×10^{-2} | 3.0197×10^{-3} | 7.3140×10^{-4} |

are the same as adopted in the previous example. The analytical solution is

$$u = \frac{T_1 \sin \beta X_2}{\sqrt{k} \sin \beta X_2} + \frac{2T_1}{\sqrt{k}} \sum_{n=1}^{\infty} \frac{n\pi \cos n\pi}{n^2\pi^2 - \beta^2 L^2} \times \sin \frac{n\pi X_2}{L} e^{-\left(\frac{n^2\pi^2}{L^2} - \beta^2\right)nt}, \tag{53}$$

where

$$T_1 = \sqrt{k_0}(\cos \beta L + 2 \sin \beta L)T. \tag{54}$$

The temperature distribution along X_2 -axis at different times is plotted in Fig. 11. The numerical results match those given by the analytical method very well.

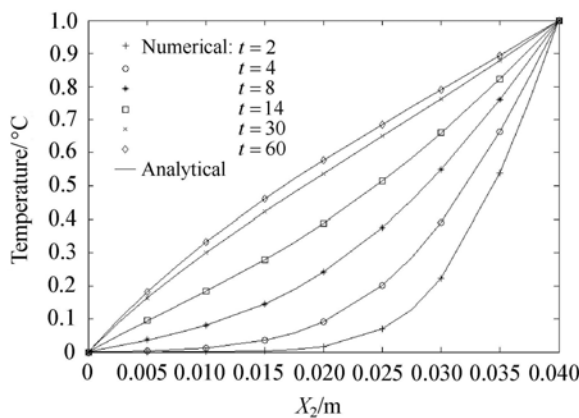


Fig. 11 Temperature distribution along X_2 at different times for the trigonometrically graded plate

Table 4 shows the results of the study of its sensitivity to mesh distortion. The results exhibit its remarkable insensitivity to mesh distortion.

Table 4 Comparison of temperature for distorted (e and z are shown in Fig. 12) and undistorted 4×4 element mesh along X_2 -axis

| X_2 | Undistorted | Distorted for $e = 0.4z$ | Distorted for $e = 0.3z$ | Analytical result |
|-------|-------------|--------------------------|--------------------------|-------------------|
| 0.01 | 0.3312 | 0.3300 | 0.3286 | 0.3320 |
| 0.02 | 0.5773 | 0.5756 | 0.5744 | 0.5776 |
| 0.03 | 0.7903 | 0.7915 | 0.7939 | 0.7903 |

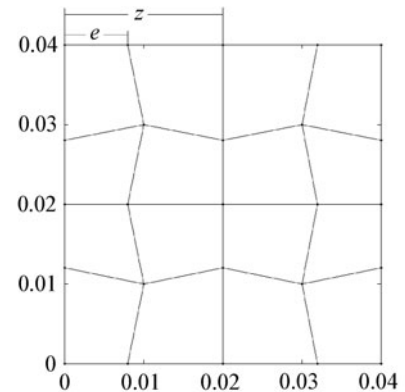


Fig. 12 Distorted mesh for Example 4

Example 5

The last numerical example is an L-shaped FGMs domain. The geometry and boundary conditions are shown in Fig. 13. $k = k_0 e^{2\beta X_2}$, $c = c_0 e^{2\beta X_2}$, $k_0 = 17 \text{ W}/(\text{m}\cdot\text{K})$, $c_0 = 1.0 \text{ MJ}/(\text{kg}\cdot\text{K})$, $\beta = 25$ are used in the calculation. The domain is discretized with 12 elements. For verification purposes, the results are compared with those obtained from conventional finite element simulation performed by the commercially available software ANSYS. With ANSYS, homogeneous elements with constant properties at the element level are used and the material gradient is achieved by a highly refined mesh with 300 elements (see Fig. 14). Contour plots of the temperature distribution at different times, as determined by the proposed model and by ANSYS, are shown in Fig. 15. Table 5 compares the temperatures at the interested points, A, B, C (see Fig. 13), given by the proposed hybrid graded element model (HGEM) and by ANSYS at different times. Good agreement can be observed between the results of proposed model and ANSYS, in which only 12 elements are used in the proposed model.

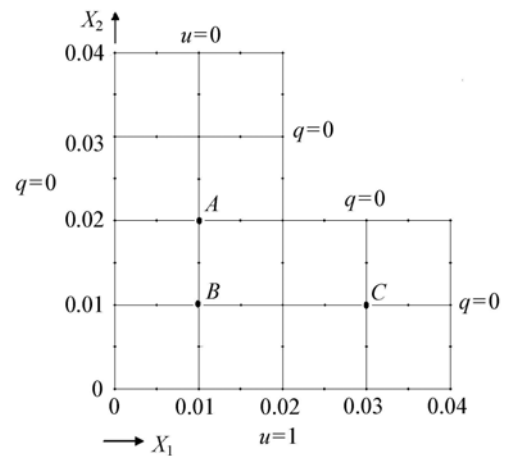


Fig. 13 L-shaped functionally graded plate and boundary condition

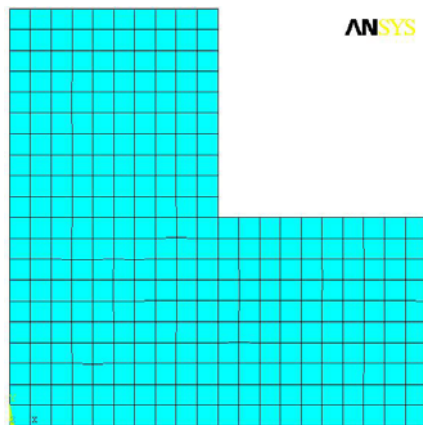


Fig. 14 The FEM mesh in ANSYS

6 Conclusions

In this paper the LT and graded element model are employed to deal with the transient heat conduction in FGMs. A fundamental solution is derived and a graded element model is developed in Laplace space. In the model, the graded element, which incorporates the material property gradient at the element level, is presented in the internal element domain. A linear combination of the fundamental solution at points outside the element domain is used to approximate the field variable in the internal element domain, and boundary interpolation functions are used to construct the frame field. Five typical examples are considered to assess the performance of the proposed method. The results show that the

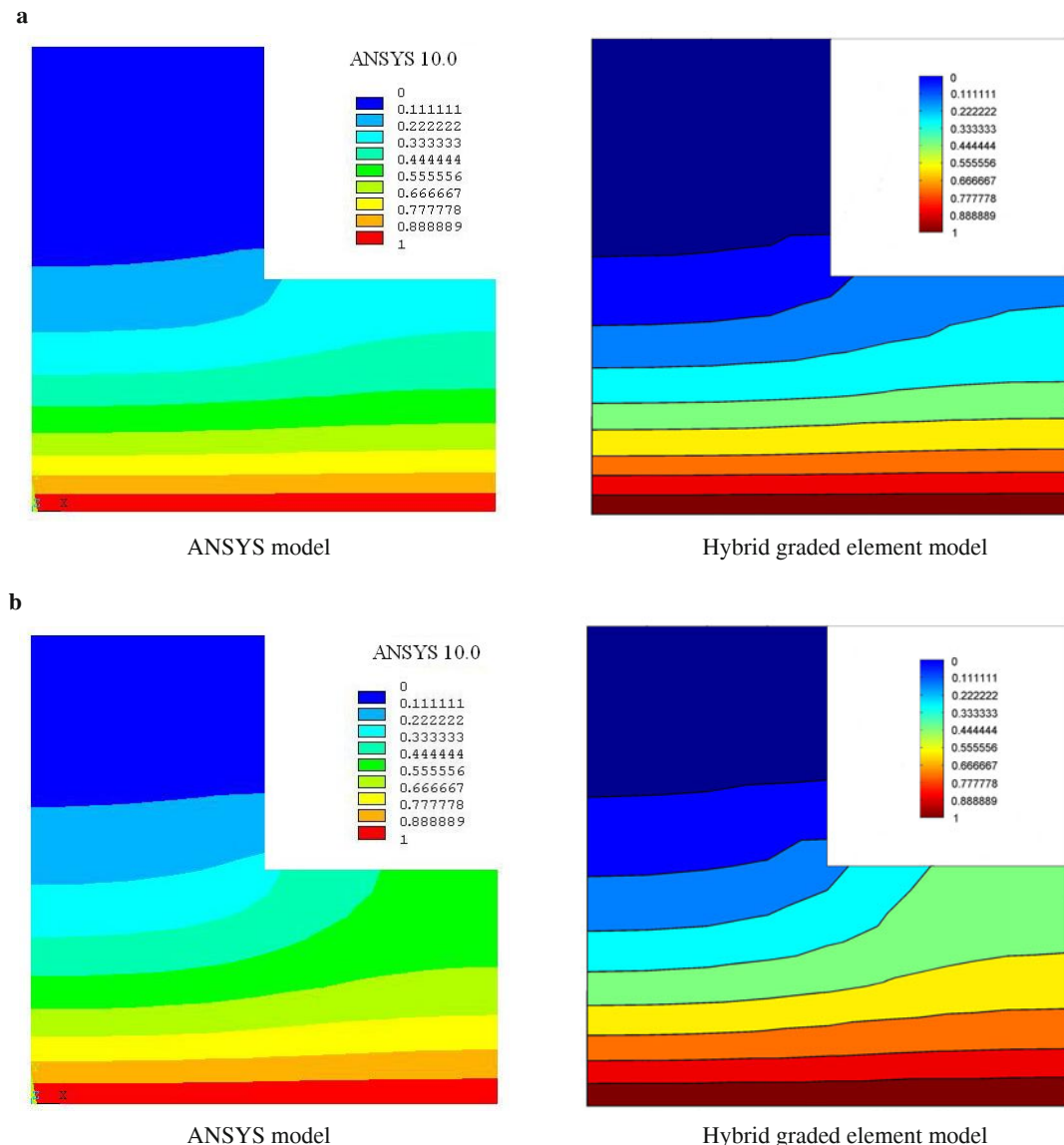


Fig. 15 Contour plots of the temperature distribution at different times by two models. **a** $t = 8$ s; **b** $t = 13$ s; **c** $t = 20$ s; **d** $t = 30$ s; **e** $t = 60$ s

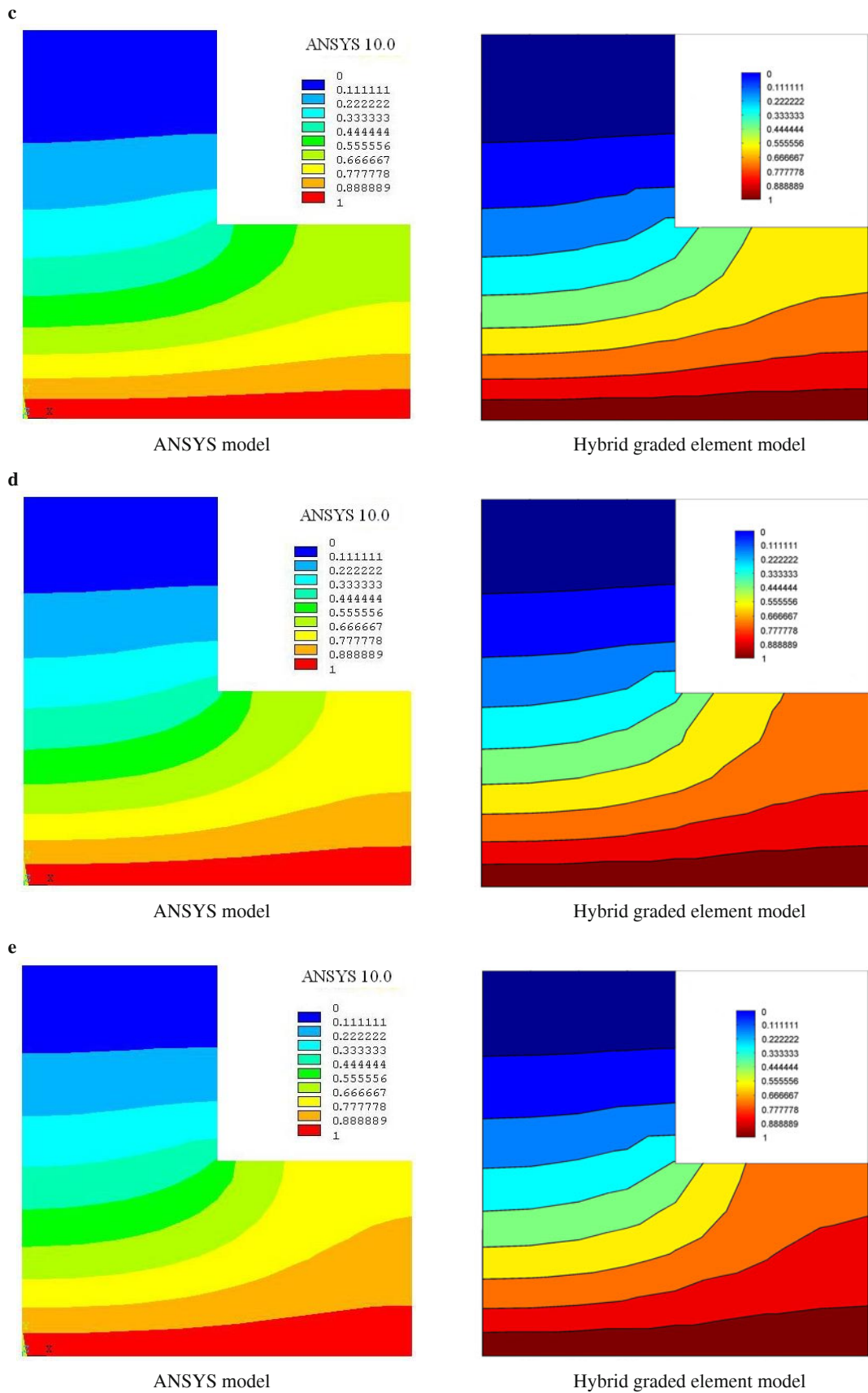


Fig. 15 Contour plots of the temperature distribution at different times by two models. **a** $t = 8$ s; **b** $t = 13$ s; **c** $t = 20$ s; **d** $t = 30$ s; **e** $t = 60$ s (continued)

Table 5 Comparison of results at the interested points

| | $t = 8 \text{ s}$ | | $t = 13 \text{ s}$ | | $t = 20 \text{ s}$ | | $t = 30 \text{ s}$ | | $t = 60 \text{ s}$ | |
|----------------|-------------------|--------|--------------------|--------|--------------------|--------|--------------------|--------|--------------------|--------|
| | HGEM | ANSYS | HGEM | ANSYS | HGEM | ANSYS | HGEM | ANSYS | HGEM | ANSYS |
| A (0.01, 0.02) | 0.1397 | 0.1321 | 0.2150 | 0.2058 | 0.2768 | 0.2681 | 0.3178 | 0.3113 | 0.3433 | 0.3392 |
| B (0.01, 0.01) | 0.4182 | 0.4062 | 0.4953 | 0.4873 | 0.554 | 0.5482 | 0.5925 | 0.5889 | 0.6164 | 0.6151 |
| C (0.03, 0.01) | 0.4655 | 0.4537 | 0.5883 | 0.5776 | 0.6844 | 0.6764 | 0.7459 | 0.7416 | 0.7827 | 0.7825 |

proposed method is efficient and accurate for transient heat conduction in FGMs. In particular, it is insensitive to the mesh distortion. Moreover, the graded element model can capture the graded character of FGMs at element level and simulates the graded material in a natural way.

References

- Zhu, S., Satravaha, P., Lu, X.: Solving linear diffusion equations with the dual reciprocity method in Laplace space. *Eng. Anal. Boundary Elem.* **13**(1), 1–10 (1994)
- Sutradhar, A., Paulino, G.H., Gray, L.J.: Transient heat conduction in homogeneous and non-homogeneous materials by the Laplace transform Galerkin boundary element method. *Eng. Anal. Boundary Elem.* **26**(2), 119–132 (2002)
- Alibeigloo, A.: Exact solution for thermo-elastic response of functionally graded rectangular plates. *Composite Struct.* **92**(1), 113–121 (2010)
- Gray, L.J., Kaplan, T., Richardson, J.D., et al.: Green's functions and boundary integral analysis for exponentially graded materials: heat conduction. *J. Appl. Mech.* **70**(4), 543–549 (2003)
- Berger, J.R., Martin, P.A., Mantić V., et al.: Fundamental solutions for steady-state heat transfer in an exponentially graded anisotropic material. *Z. Angew. Math. Phys. (ZAMP)* **56**(2), 293–303 (2005)
- Paulino, G., Sutradhar, A., Gray, L.: Boundary element methods for functionally graded materials. *Boundary Elem. Tech.* **15**, 137–146 (2003)
- Sutradhar, A., Paulino, G.H.: The simple boundary element method for transient heat conduction in functionally graded materials. *Comput. Meth. Appl. Mech. Eng.* **193**(42–44), 4511–4539 (2004)
- Sladek, J., Sladek, V., Zhang, C.: Transient heat conduction analysis in functionally graded materials by the meshless local boundary integral equation method. *Comput. Mater. Sci.* **28**(3–4), 494–504 (2003)
- Sladek, V., Sladek, J., Tanaka, M., et al.: Transient heat conduction in anisotropic and functionally graded media by local integral equations. *Eng. Anal. Boundary Elem.* **29**(11), 1047–1065 (2005)
- Marin, L.: Numerical solution of the Cauchy problem for steady-state heat transfer in two-dimensional functionally graded materials. *Int. J. Solids Struct.* **42**(15), 4338–4351 (2005)
- Marin, L., Lesnic, D.: The method of fundamental solutions for nonlinear functionally graded materials. *Int. J. Solids Struct.* **44**(21), 6878–6890 (2007)
- Wang, H., Qin, Q.H., Kang, Y.: A meshless model for transient heat conduction in functionally graded materials. *Comput. Mech.* **38**(1), 51–60 (2006)
- Anlas, G., Santare, M.H., Lambros, J.: Numerical calculation of stress intensity factors in functionally graded materials. *Int. J. Fract.* **104**(2), 131–143 (2000)
- Li, H., Lambros, J., Cheeseman, B.A., et al.: Experimental investigation of the quasi-static fracture of functionally graded materials. *Int. J. Solids Struct.* **37**(27), 3715–3732 (2000)
- Gu, P., Dao, M., Asaro, R.J.: A simplified method for calculating the crack-tip field of functionally graded materials using the domain integral. *J. Appl. Mech.* **66**(1), 101–108 (1999)
- Santare, M.H., Lambros, J.: Use of graded finite elements to model the behavior of nonhomogeneous materials. *J. Appl. Mech.* **67**(4), 819–822 (2000)
- Kim, J.H., Paulino, G.H.: Isoparametric graded finite elements for nonhomogeneous isotropic and orthotropic materials. *J. Appl. Mech.* **69**(4), 502–514 (2002)
- Wang, H., Qin, Q.H.: Hybrid FEM with fundamental solutions as trial functions for heat conduction simulation. *Acta Mech. Solida Sinica* **22**(5), 487–498 (2009)
- Qin, Q.H.: Hybrid-Trefftz finite element method for Reissner plates on an elastic foundation. *Comput. Meth. Appl. Mech. Eng.* **122**(3–4), 379–392 (1995)
- Qin, Q.H.: Nonlinear analysis of Reissner plates on an elastic foundation by the BEM. *Int. J. Solids Struct.* **30**(22), 3101–3111 (1993)
- Qin, Q.H.: *Trefftz Finite and Boundary Element Method*. WIT Press, Southampton (2000)
- Qin, Q.H.: *MATLAB and C Programming for Trefftz Finite Element Methods*. CRC Press, Taylor & Francis (2008)
- Qin, Q.H.: Hybrid Trefftz finite-element approach for plate bending on an elastic foundation. *Appl. Math. Model* **18**(6), 334–339 (1994)
- Carslaw, H.S., Jaeger, J.C.: *Conduction of Heat in Solids*. Oxford University Press, Oxford, 1986
- Qin, Q.H.: Variational formulations for TFEM of piezoelectricity. *Int. J. Solids Struct.* **40**(23), 6335–6346 (2003)
- Davies, B., Martin, B.: Numerical inversion of the Laplace transform—A survey and comparison of methods. *J. Comput. Phys.* **33**, 1–32 (1979)